PHYSICAL REVIEW A VOLUME 51, NUMBER 2 FEBRUARY 1995

Comparative study of exchange-correlation effects on the electronic and optical properties of alkali-metal clusters

M. Madjet and C. Guet
Commissariat à l'Energie Atomique, Département de Recherche Fondamentale sur la Matière Condensée, Laboratoire des Ions, Atomes et Agrégats, 17, rue des Martyrs, F38054 Grenoble Cedex 9, France

W.R. Johnson
Department of Physics, University of Notre Dame, Notre Dame, Indiana 46556
(Received 3 May 1994; revised manuscript received 11 October 1994)

Ground-state properties of alkali-metal clusters are investigated within the framework of the jellium model from the standpoint of either the local-density approximation of the density-functional theory or the nonlocal Hartree-Fock theory. Accordingly, the optical response is calculated microscopically within the corresponding time-dependent theory. The present study deals with closed-shell systems with up to 200 delocalized electrons. A comparative investigation of various approximations is carried out. In spite of significantly different mean-field potentials, a consistent inclusion of polarization-type many-body effects leads to surprisingly similar theoretical predictions of the first moments of the oscillator strength distribution. This agreement is discussed in terms of sum-rule constraints. The remaining discrepancies with regard to the measured data originate from the jellium assumption which underlies our calculations.

PACS number(s): 31.10.+z, 31.25.Qm, 36.40.+d

I. INTRODUCTION

The optical response of alkali-metal clusters has been now measured for a large variety of systems [1–7]. The energy dependence of the photoabsorption cross section of clusters with filled electronic shells is particularly simple and observed as a broad resonance around a frequency which is typical of the corresponding bulk metal. This has lead quickly to an interpretation in terms of the so-called jellium model. In this model, the electron-nucleus many-body problem is reduced to that for a system of delocalized valence electrons, the neutralization being ensured by an uniform positively-charged background, the density of which is a parameter that is usually chosen to be the bulk density.

Various theoretical approaches to dealing with the response of the finite electron system to an external dipole field have been considered. They are all variants of the random-phase approximation (RPA) to the theory of small amplitude vibrations of a finite fermion system. The time-dependent local-density approximation (TDLDA) formalism, which had gained success in the context of atomic photoionization [8], was extended to jellium metal spheres [9,10]. Prior to any relevant data, it predicted quite nicely both static polarizabilities and dipole absorption frequencies. It already appeared that the polarization effects arising from many-body correlations were indeed important and thus necessary to give the correct absorption resonance. Alternatively, one may treat this collective effect through a matrix formulation of the RPA [11–13] which, although computationally more demanding, allows one to consider nonlocal interactions [14]. Simpler approximations to the full RPA such as the semiclassical RPA sum rule [15] and the local RPA [16] have also been used.

All of the works mentioned previously, except that of Ref. [14], were based on the LDA, i.e., it was assumed that the exchange and correlation contributions should be treated on an equal footing, albeit locally, and thus cast into a local density-dependent potential. The subsequent construction of the ground state is then easily performed within an effective mean-field theory. For bulk metal, the LDA is indeed a much more natural approximation than the Hartree-Fock (HF) approximation, which fails to provide a finite density of states at the Fermi energy. However, for finite systems, the superiority of the LDA has yet to be established. Apart from inhomogeneity effects, which can be treated by a gradient expansion formalism, the LDA fails to provide the expected asymptotic falloff of the mean-field potential that an electron sees. By contrast, the HF potential has the correct $1/r$ asymptotic behavior since the Fock exchange term compensates for the fact that an electron does not interact with itself. Moreover, the HF theory is the natural framework for including correlation effects in many-body perturbation theory.

It was observed that theoretical polarizabilities calculated within the LDA framework were systematically lower than measured polarizabilities and that, consistently, the predicted dipole resonance frequencies were blueshifted with respect to the experimental data. It was conjectured that this defect might originate from the incorrect asymptotic behavior of the potential which could crucially affect those observables that are sensitive to outer parts of the wave function, such as dipole transitions. This was indeed the motivation of our previous work [14]: to calculate the dipole vibrations within the framework of the random-phase approximation with exchange (RPAE), and to show eventually that the exact treatment of exchange does not resolve the discrepancies

with the experimental data. Note also that within the framework of the LDA, some recipes exist to correct for the self-interaction [17], and that a clear improvement has been claimed in some recent works [18].

In the present paper, we report a systematic comparative study of an exact treatment of exchange correlations versus local treatments. The ground state is described either in the HF approximation, leading to a nonlocal HF central potential or in the LDA by solving the Kohn-Sham equations. In both cases, a complete basis of single-particle states is constructed by confining the cluster to a cavity of large but finite radius, thereby discretizing the continuum. The spectrum of physical dipole-excited states is then obtained by solving either the RPAE or the RPA matrix equation. These states are used to determine oscillator strengths for dipole transitions from the ground state as well as the ground-state static dipole polarizability. An assessment of our approximation for the continuum states within the matrix RPA formulation is done by comparing to a TDLDA calculation similar to that worked out by Bertsch [19]. Unless specified otherwise, we use atomic units.

II. HARTREE-FOCK AND LDA GROUND STATES OF JELLIUM CLUSTERS

In the jellium model an alkali-metal cluster consists of itinerant electrons, one electron per atom, in a positively-charged uniform background. This uniform background has been implicitly obtained through a convolution of a smooth ionic distribution with an electron-ion potential that merely equals $-\frac{1}{r}$, thus disregarding any ionic structure effect. In the following, we shall assume the electron density to be spherically symmetric. This assumption is likely to be well justified for clusters with a number of valence electrons (8, 18, 20, 34, 40, 58, 92,...) that form a closed shell in a spherical potential. The many-body jellium Hamiltonian, describing the system made of Z delocalized electrons in the presence of A ions, is expressed as

$$H_J = \sum_i^Z \frac{\mathbf{p}_i^2}{2} + V_{\rm bkg}(r_i) + \frac{1}{2}\sum_{i,j}^Z \frac{1}{|\mathbf{r}_i - \mathbf{r}_j|}\,, \qquad (2.1)$$

where $V_{\rm bkg}(r)$ is the positively-charged background potential. For a constant-density distribution for the A ions, the background potential is given by

$$V_{\rm bkg}(r) = \begin{cases} -\frac{A}{2R}\left[3 - \left(\frac{r}{R}\right)^2\right], & r \le R \\ -\frac{A}{r}, & r > R, \end{cases} \qquad (2.2)$$

where $R = A^{\frac{1}{3}} r_S$. The Wigner-Seitz radius r_S is assigned its bulk value, i.e., $4a_0$ for sodium (a_0 being the Bohr radius). The many-body Hamiltonian is separated into a model independent-particle Hamiltonian H_0 and the residual two-body interaction V_r:

$$H_J = H_0 + V_r\,, \qquad (2.3)$$

$$H_0 = \sum_{i=1}^Z h_0(r_i), \qquad (2.4)$$

where the one-electron operator

$$h_0 = \frac{1}{2}p^2 + V_{\rm bkg}(r) + U(r)\,, \qquad (2.5)$$

contains the mean-field potential $U(r)$ which accounts in some approximation for the electron-electron interaction.

In the HF theory, the ground state is approximated by a Slater determinant of single-particle wave functions and the Ritz variational principle is invoked to derive the HF equations and the HF potential. The HF potential [$U(r)$ in Eq. (2.5)] is the sum of a direct and a nonlocal exchange terms. The nonlocal contribution is essential; it corrects naturally for the fact that an electron does not interact with itself and leads to the physically correct asymptotic behavior, $\frac{Z-1}{r}$, of the mean-field potential.

In the density-functional theory (DFT), according to the Hohenberg-Kohn theorem, [20] the ground-state energy is a minimum for the exact density of a functional of the density. In the spirit of the DFT, Kohn and Sham proposed a self-consistent-field method which takes into account approximatively exchange and correlation effects. The method leads for the ground state to a set of self-consistent equations analogous to the Hartree equations. It amounts to writing the potential U of Eq. (2.5) as the sum of the direct Hartree potential and a density-dependent local exchange-correlation potential, $V_{\rm xc}[\rho(\mathbf{r})]$. In order to be consistent with previous works [21], we use the local-density approximation (LDA) exchange-correlation energy density $\epsilon_{\rm xc}$ of Gunnarsson and Lundqvist [22] which is expressed as

$$\epsilon_{\rm xc} = -\frac{3}{4}\left(\frac{9}{4\pi^2}\right)^{1/3}\frac{1}{r_S(\mathbf{r})} - 0.0333\, G\Big(r_S\left(\frac{\mathbf{r}}{11.4}\right)\Big),$$
$$G(x) = (1+x^3)\ln\left(1+\frac{1}{x}\right) - x^2 + \frac{x}{2} - \frac{1}{3}\,, \qquad (2.6)$$

where $r_S(\mathbf{r}) = [\frac{3}{4\pi\rho(\mathbf{r})}]^{1/3}$ is the local Wigner-Seitz radius. This leads to

$$V_{\rm xc}(\mathbf{r}) = \frac{\delta[\rho(\mathbf{r})\epsilon_{\rm xc}(\rho(\mathbf{r}))]}{\delta\rho(\mathbf{r})}$$
$$= -\left(\frac{9}{4\pi^2}\right)^{1/3}\frac{1}{r_S(\mathbf{r})} - 0.0333\ln\left(1+\frac{11.4}{r_S(\mathbf{r})}\right). \qquad (2.7)$$

Note that the first term on the right-hand side of Eq. (2.7) is exactly the exchange potential derived variationally from the HF exchange energy of a uniform electron liquid, immersed in a uniform background of positive charge. In order to compare this to the exact HF potential for finite systems, it is natural to consider this exchange potential rather than the Slater exchange potential [23], which is a factor $\frac{3}{2}$ larger in magnitude. Asymptotically, the density-dependent potential of Eq. (2.7) behaves as $\rho(\mathbf{r})^{1/3}$, i.e., exponentially.

The self-interaction correction (SIC) to restore the correct $\frac{Z-1}{r}$ asymptotic behavior was considered within the framework of the LDA by Perdew and Zunger [17] and applied to metallic clusters [24,18]. In the SIC approximation, the state-dependent Kohn-Sham (KS) single-

particle potential is written as

$$V^a_{\rm SIC}(\mathbf{r}) = \int \frac{[\rho(\mathbf{r}') - \rho_a(\mathbf{r}')]}{|\mathbf{r}-\mathbf{r}'|} d\mathbf{r}' + V_{\rm xc}(\rho(\mathbf{r})) - V_{\rm xc}(\rho_a(\mathbf{r}))\,, \quad (2.8)$$

where $\rho_a(\mathbf{r})$ is the a single-particle state density,

$$\rho_a(\mathbf{r}) = u^\dagger_a(\mathbf{r}) u_a(\mathbf{r})\,. \quad (2.9)$$

Restricting the discussion to spherically symmetric closed-shell systems, $u_{nlm}(\mathbf{r}) = \frac{R_{nl}(r)}{r} Y_{lm}(\theta,\phi)\chi$, and depending on whether we treat exchange exactly or use the LDA, we are led to solve either coupled radial HF equations or coupled radial KS equations for the occupied orbitals:

$$\left[-\frac{1}{2}\frac{d^2}{dr^2} + V_{\rm bkg}(r) + U(r) + \frac{l(l+1)}{2r^2}\right] R_{nl}(r) = \epsilon_{nl} R_{nl}(r)\,. \quad (2.10)$$

Numerical comparisons

Our numerical codes yield single-particle radial orbitals $R_{nl}(r)$ and eigenenergies ϵ_{nl} to a very high accuracy (typically one part in 10^8). The HF calculations have been carried out for clusters with up to 200 particles, whereas the KS calculations can be performed for much larger systems.

In order to assess the validity of the LDA, we compare HF predictions of ground-state properties to predictions obtained within the LDA with only a local exchange term (denoted as LDAX). Such a comparison has already been done for clusters with up to 58 delocalized electrons by Hansen and Nishioka [25]. The present calculations that extend to larger systems reach the same conclusions as Ref. [25]. In the upper panel of Fig. 1, we show the ground-state electronic densities $\rho_{\rm HF}(r)$ and $\rho_{\rm LDAX}(r)$ for a closed-shell system of 92 particles with $r_S = 4a_0$, calculated within the HF approximation and LDAX, respectively. These two density profiles coincide almost perfectly in the surface and in the tail region. The LDA shows less pronounced quantal oscillations in the inner part of the cluster than does the HF approximation.

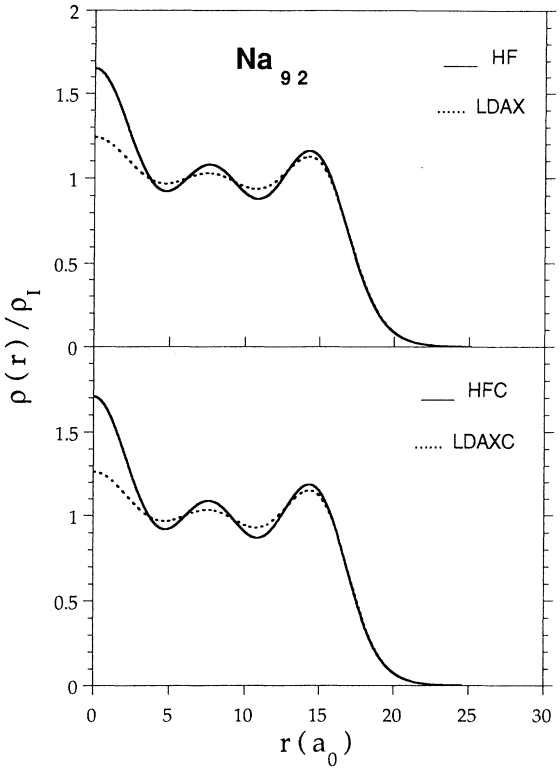

FIG. 1. Radial electronic density of Na_{92} ($r_S = 4a_0$), $\rho(r)$, normalized to the constant positively charged density, ρ_I. Top panel: Hartree-Fock versus local-density approximation with only exchange interaction. Bottom panel: Hartree-Fock plus density-dependent correlation versus local-density approximation with exchange-correlation interaction.

The second moments of the radial density are reported in Table I for a set of closed-shell systems (8, 20, 34, 40, 58, 92, 138, 196). The agreement between the HF and LDA predictions is surprisingly good. The difference is already less than 1% for 20 particles and is negligible (one part in 10^4) for 196 particles.

The excellent agreement for densities is also observed for total ground-state energies as shown in Table II. Whereas the total energies differ by about 1% for eight

TABLE I. Second moment $\langle r^2 \rangle$ (a_0^2) of the valence electron density of Na clusters ($r_S = 4a_0$) for different sizes A, calculated in the Hartree-Fock approximation (HF), in the Hartree-Fock approximation with correlation (HFC), and in the Kohn-Sham approximation either with exchange only (LDAX) or with exchange correlation (LDAXC). Hartree-Fock self-interaction corrected predictions are also given (LDAX-SIC and LDAXC-SIC). See text.

$A=$	8	20	34	40	58	92	138	196
HF	44.11	76.85	106.24	118.82	149.26	201.13	262.05	329.73
LDAX	44.71	77.17	106.60	118.95	149.54	201.34	262.19	329.83
LDAX-SIC	43.51	76.52	106.33	118.58	149.40	201.28	262.16	329.85
LDAXC	42.84	75.31	104.84	117.07	147.82	199.63	260.46	328.09
LDAXC-SIC	42.95	75.80	105.48	117.72	148.50	200.33	261.17	328.81
HFC	42.34	75.06	104.54	116.99	147.59	199.47	260.37	328.03

TABLE II. Total energy (a.u.) of valence electrons in Na clusters ($r_S = 4a_0$) for different sizes A, calculated in the Hartree-Fock approximation (HF), in the Hartree-Fock approximation with correlation (HFC), and in the Kohn-Sham approximation either with exchange only (LDAX) or with exchange correlation (LDAXC). Hartree-Fock self-interaction corrected predictions are also given (LDAX-SIC and LDAXC-SIC). See text.

$A=$	8	20	34	40	58	92	138	196
HF	5.18	23.01	55.07	71.94	133.00	285.42	559.02	1000.82
LDAX	5.11	22.90	54.89	71.78	132.75	285.10	558.64	1000.37
LDAX-SIC	5.28	23.20	55.31	72.23	133.32	285.84	559.56	1001.48
LDAXC	5.38	23.59	56.09	73.19	134.82	288.41	563.63	1007.48
LDAXC-SIC	5.38	23.53	55.96	73.09	134.56	287.95	562.91	1006.45
HFC	5.45	23.71	56.28	73.35	135.08	288.73	564.00	1007.92

particles, they agree with each other to better than one part in 10^3 for systems with more than 92 particles. These results on ground-state energies and densities confirm the validity of the functional theory. In the present case where only exchange is taken into account, the exchange energy density is perfectly well known so that for a homogeneous large system an exact agreement should be obtained. The tiny differences that we observe are due to the quantum finite-size effects which are indeed playing a role only in the inner region where the potential acts.

The good agreement on ground-state energies and densities should not, however, mask the marked differences in the self-consistent mean-field potentials that the HF approximation and the LDAX provide. As an illustration, we show in Fig. 2 the LDAX mean-field potential seen by an electron of Na_{92}. In the same figure, we have also plotted the state-dependent HF potentials seen by a $1s$ and a $1h$ electron. As discussed above, the HF potentials behave asymptotically as $-\frac{1}{r}$, thus being much shallower in the outer region than the LDA potential which falls off exponentially. The LDAX potential is less attractive than the HF potential also in the inner part leading to a spectrum of single-particle state eigenenergies systematically higher than the HF spectrum. These eigenenergies are reported in Table III for the ten filled orbitals of Na_{92}.

The density-functional theory treats exchange and correlation interactions on an equal footing. Starting from the HF theory, it is a major task to include the correlation contributions to the ground-state wave function through configuration interaction methods or many-body perturbation theory. Some work along these lines has already been published [26–28]. In the present paper, we consider a hybrid model which we shall denote by HFC (Hartree-Fock plus correlation) in which the correlation contribution is just the same as in the LDA. Using this *ad hoc* prescription, we have assumed that the nonlocality is entirely in the exchange term that we treat exactly. For clarity, let us denote the LDA with exchange and correlation by LDAXC.

In the lower panel of Fig. 1, we show the densities of Na_{92} now obtained in the LDAXC and in the HFC approximation. As expected these two densities differ from each other only in the inner region. The interesting point is that the inclusion of a correlation term in the energy density functional does not lead to any sensitive change of the density. This fact can be checked by comparing the second moment of the density as shown in Table I. For the smallest eight-particle cluster the correlation part of the Gunnarsson-Lundkvist functional, Eq. (2.7), brings a reduction of the root mean square radius of about 2%. This volume contraction due to correlation, however, quickly diminishes with size: for 40 particles the rms radii differ already by less than 1%. Thus, for medium-large clusters, the four different approximations provide very similar densities.

An inspection of the values reported in Table II shows that the total ground-state energies per particle are lowered by about 0.96 eV per particle, very close to the 1.02 eV correlation contribution to the energy density of Eq. (2.6) that is obtained for $r_S = 4a_0$. As a matter of fact, the effect of the correlation potential comes down to an almost constant shift of about 0.9 eV for the eigenenergies of all single-particle states. This can be seen from Table III for Na_{92}. Note that the wave functions are not significantly modified. The fact that the correlation potential just shifts the eigenenergy spectrum arises from its

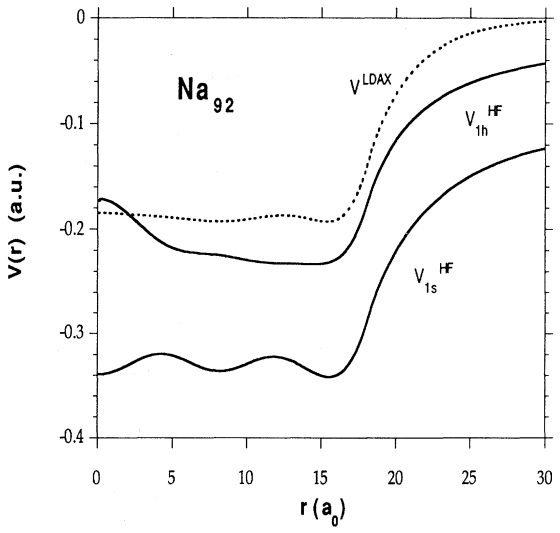

FIG. 2. Radial mean-field electronic potential, $V(r)$ (a.u.) for Na_{92} ($r_S = 4a_0$). Hartree-Fock potentials seen by the $1s$-state and $1h$-state electrons versus local-density approximation with only exchange interaction (LDAX).

TABLE III. Energy parameter (eV) of the occupied single-particle states of the A=92 closed-shell jellium cluster ($r_S = 4a_0$) calculated in the Hartree-Fock approximation (HF), in the Hartree-Fock approximation with correlation (HFC), and in the Kohn-Sham approximation either with exchange only (LDAX) or with exchange correlation (LDAXC). Hartree-Fock self-interaction corrected predictions are also given (LDAX-SIC and LDAXC-SIC). See text.

nl =	1s	1p	1d	2s	1f	2p	1g	2d	3s	1h
HF	-8.65	-8.04	-7.23	-6.81	-6.23	-5.52	-5.00	-3.79	-3.50	-3.38
LDAX	-4.84	-4.49	-4.05	-3.85	-3.54	-3.23	-2.95	-2.52	-2.31	-2.29
LDAX-SIC	-6.02	-5.48	-4.96	-4.89	-4.40	-4.20	-3.77	-3.42	-3.29	-3.08
LDAXC	-5.69	-5.35	-4.92	-4.70	-4.41	-4.08	-3.83	-3.36	-3.17	-3.13
LDAXC-SIC	-6.48	-6.02	-5.53	-5.44	-4.97	-4.74	-4.35	-3.95	-3.79	-3.65
HFC	-9.51	-8.92	-8.13	-7.69	-7.13	-6.39	-5.91	-4.64	-4.34	-4.28

simple functional form given by Eq. (2.7). Since the log function of the third power of the total density does not vary appreciably over the radial extent of single-particle wave functions, we expect from perturbation theory a constant shift for all occupied states.

A quantity of interest for further discussions is the spillout length which can be expressed as

$$\delta_e = \frac{1}{3}\frac{\Delta Z}{Z^{2/3}} r_S \,, \tag{2.11}$$

where ΔZ measures the number of electrons in the ground state that are outside the jellium sphere:

$$\Delta Z = \int_R^\infty \rho(\mathbf{r}) d\mathbf{r} \,. \tag{2.12}$$

In harmony with the moment analysis of the density distribution, the electron spillout length, which is listed in Table IV for clusters of various sizes, is slightly overestimated by the LDAX with respect to the exact HF prediction. Note again that the discrepancy is vanishingly small as the cluster size increases. The spillout length is reduced by about 10% when the correlation is switched on, due to the contraction of the density. The magnitude of the electronic spillout is found to be rather independent of size and equal around 0.55 a_0 for $r_S = 4a_0$.

Local-density approximation calculations including the self-interaction correction (SIC) have also been performed for the present closed-shell systems. Since the state-dependent LDAX-SIC potential is close to the HF potential, the single-particle energy parameters are in better agreement than in the LDAX case (see Table III). With regard to the ground-state densities, we observe that for large systems the LDAX-SIC leads to even a larger electronic volume than the LDAX, whereas for the smaller systems (Z = 8, 20) it underestimates the electronic spatial extent. Keep in mind, however, that all these discrepancies are small. Whereas the LDAX would yield binding energies that are systematically higher than the HF binding energies, the SIC prescription overestimates the correction leading to a systematic overbinding of the jellium clusters (see Table II).

III. OPTICAL RESPONSE

The response of a metallic jellium cluster to a time-dependent external electromagnetic field of frequency ω, which amounts to its dipole contribution since the cluster radius is much smaller than the relevant radiation wavelength, is revealed by the photoabsorption spectrum. In a linear response approximation, the deviation from the unperturbed density which we denote by $\delta\rho(\mathbf{r};\omega)$ is related to the weak external field, $V_{\rm ext}(\mathbf{r};\omega)$, by

$$\delta\rho(\mathbf{r},w) = \int d\mathbf{r}' \chi(\mathbf{r},\mathbf{r}';\omega) V_{\rm ext}(\mathbf{r}';\omega) \,, \tag{3.1}$$

where $\chi(\mathbf{r},\mathbf{r}';\omega)$ is the nonlocal frequency dependent susceptibility. The induced charge displacement will in turn give rise to an induced dipole moment and a complex, frequency dependent, dipole polarizability, $\alpha(\omega)$, that can

TABLE IV. Spillout length δ (a_0) of the valence-electron density of Na clusters ($r_S = 4a_0$) for different sizes A, calculated in the Hartree-Fock approximation (HF), in the Hartree-Fock approximation with correlation (HFC), and in the Kohn-Sham approximation either with exchange only (LDAX) or with exchange correlation (LDAXC). Hartree-Fock self-interaction corrected predictions are also given (LDAX-SIC and LDAXC-SIC). See text for definition.

A =	8	20	34	40	58	92	138	196
HF	0.525	0.567	0.521	0.603	0.528	0.542	0.562	0.576
LDAX	0.544	0.574	0.541	0.603	0.545	0.555	0.570	0.580
LDAX-SIC	0.518	0.571	0.552	0.609	0.560	0.571	0.587	0.598
LDAXC	0.486	0.519	0.485	0.548	0.490	0.501	0.516	0.527
HFC	0.471	0.523	0.478	0.560	0.487	0.501	0.521	0.534
LDAXC-SIC	0.500	0.550	0.526	0.586	0.532	0.544	0.560	0.571

be expressed as

$$\alpha(\omega) = -e^2 \sum_k \left[\frac{|\langle k|\sum_i z_i|0\rangle|^2}{\hbar\omega - (E_k - E_0) + i\delta} - \frac{|\langle k|\sum_i z_i|0\rangle|^2}{\hbar\omega + (E_k - E_0) + i\delta} \right], \quad (3.2)$$

where we have assumed the external electric field to be in the z direction and used the length form for the dipole operator. Note that $|0\rangle$ is the exact many-body ground state. The knowledge of the dipole dynamical polarizability allows one to determine the photoabsorption cross section in terms of the imaginary part of the polarizability using the relation

$$\sigma(\omega) = 4\pi \frac{\omega}{c} \mathrm{Im}[\alpha(\omega)] \quad (3.3)$$

and, incidentally, the static dipole polarizability by setting $\omega = 0$ in Eq. (3.2). One can express the photoabsorption cross section as

$$\sigma(E) = 2\pi^2 \frac{e^2\hbar}{mc} \sum_k f_k \delta(E - E_k + E_0), \quad (3.4)$$

in terms of the oscillator strengths f_k for the transition from the ground state to the kth excited state that are defined as

$$f_k = \frac{2m\omega}{\hbar} |\langle k|z|0\rangle|^2 . \quad (3.5)$$

Starting from a ground state described within an independent-particle model, there are essentially two ways of deriving the photoabsorption cross section, depending on whether the many-body physics is cast into the states or into the operator itself.

A. Time-dependent local-density approximation

In the time-dependent local-density approximation (TDLDA), one calculates directly the susceptibility by using the Green's function method. This is a very efficient method when dealing with local potentials. The integration of the self-consistent Kohn-Sham equations provides the filled orbitals and the effective Kohn-Sham potential of Eq. (2.10). The Green's functions that satisfy the differential equation,

$$\left[\frac{1}{2}\nabla^2 + E - V_{\mathrm{LDA}}\right] G(\mathbf{r},\mathbf{r}';E) = \delta(\mathbf{r}-\mathbf{r}'), \quad (3.6)$$

are obtained by numerical integration and allow one to construct the zeroth order susceptibility, $\chi_0(\mathbf{r},\mathbf{r}';\omega)$, that can be expressed as

$$\chi_0(\mathbf{r},\mathbf{r}';\omega) = \sum_{i\le f} \phi_i^*(\mathbf{r})\phi_i(\mathbf{r}')G(\mathbf{r},\mathbf{r}';\epsilon_i + \hbar\omega) + \sum_{i\le f} \phi_i(\mathbf{r})\phi_i^*(\mathbf{r}')G(\mathbf{r},\mathbf{r}';\epsilon_i - \hbar\omega). \quad (3.7)$$

The TDLDA approximation to the susceptibility is then expressed as

$$\chi(\mathbf{r},\mathbf{r}';\omega) = \chi_0(\mathbf{r},\mathbf{r}';\omega) + \chi_0(\mathbf{r},\mathbf{r}';\omega) \int d\mathbf{r}'' K(\mathbf{r},\mathbf{r}'')\chi(\mathbf{r}'',\mathbf{r}';\omega), \quad (3.8)$$

where the driving kernel, $K(\mathbf{r},\mathbf{r}')$, is just the residual interaction:

$$K(\mathbf{r},\mathbf{r}') = \frac{\delta V_{\mathrm{LDA}}(\mathbf{r})}{\delta\rho(\mathbf{r}')} = \frac{1}{|\mathbf{r}-\mathbf{r}'|} + \frac{\delta V_{\mathrm{xc}}[\rho(\mathbf{r})]}{\delta\rho(\mathbf{r}')}\delta(\mathbf{r}-\mathbf{r}'). \quad (3.9)$$

A computer code, similar to the one written by Bertsch [19], has been used in the present work to calculate the optical response within the TDLDA framework for comparison to the other approach that we shall refer to as the random-phase approximation (RPA).

B. Matrix random-phase approximation

The RPA and the TDLDA are physically equivalent approximations. In the random-phase approximation that we use here, the aim is to construct the correlated many-body excited states of Eq. (3.2). The RPA consists in diagonalizing the residual interaction of Eq. (2.3) within a model space that is restricted to one-particle–one-hole ($1p$-$1h$) excitations and linearizing the equations of motion (see, for instance, Ref. [29] for an exhaustive discussion of the method). The vibrational modes are obtained after solving the RPA matrix equation:

$$\begin{pmatrix} A & B \\ B^* & A^* \end{pmatrix} \begin{pmatrix} X^k \\ Y^k \end{pmatrix} = \omega_k \begin{pmatrix} X^k \\ -Y^k \end{pmatrix}. \quad (3.10)$$

The matrix A contains matrix elements of the residual interaction between particle-hole excitations, whereas the matrix B is composed of matrix elements of that interaction between the ground state and two-particle–two-hole excitations:

$$A_{ma,nb} = (\epsilon_m - \epsilon_a)\delta_{ab}\delta_{mn} + \langle mb|V|an\rangle,$$
$$B_{ma,nb} = \langle mn|V|ab\rangle . \quad (3.11)$$

The indices a, b (n, m) refer to the hole (particle) states. The positive eigenvalues ω_k of Eq. (3.10) are the excitation energies of the system. The corresponding eigenvectors, representing the physical states, are expressed as linear combinations of forward-going and backward-going amplitudes X^k_{ma} and Y^k_{ma} that satisfy the normalization equation:

$$\sum_{a,m} \left(|X^k_{ma}|^2 - |Y^k_{ma}|^2 \right) = 1 . \quad (3.12)$$

The transition amplitude of a one-body operator $F = \sum_{ij} a_i^\dagger a_j \langle i|f|j\rangle$ between the ground state to the kth ex-

cited state, takes then the form,

$$\langle k|F|0\rangle = \sum_{a,m} \left[X^k_{ma}\langle m|f|a\rangle + Y^k_{ma}\langle a|f|m\rangle\right] . \quad (3.13)$$

The RPA dipole matrix element of Eq. (3.2) and, therefore, the photoabsorption cross section can then be readily calculated.

In the case where the ground state has been defined as an exact HF Slater determinant, the residual interaction which enters into Eq. (3.11) is the exact Coulomb interaction with both direct and exchange parts. The p-h interaction matrix element is given by

$$\langle ij|V|kl\rangle = \left\langle ij\left|\frac{1}{|\mathbf{r}-\mathbf{r}'|}\right|kl\right\rangle - \left\langle ij\left|\frac{1}{|\mathbf{r}-\mathbf{r}'|}\right|lk\right\rangle . \quad (3.14)$$

We are then led to solve the matrix equation within the RPA with exchange (RPAE). The RPAE was developed in the context of atomic physics by Amusia and Cherepkov [30].

In the alternative case where the ground state has been defined as LDA Slater determinant the residual interaction is then that defined in Eq. (3.9), thus leading to

$$\langle ij|V|kl\rangle = \left\langle ij\left|\frac{1}{|\mathbf{r}-\mathbf{r}'|}\right|kl\right\rangle + \left\langle ij\left|\frac{\delta V_{\rm xc}}{\delta\rho}\right|kl\right\rangle . \quad (3.15)$$

We shall again consider two cases: the case where only the local exchange interaction is considered (the approximation is denoted RPAX) and the case (denoted as RPAXC) where the full exchange-correlation interaction is taken into account. The RPAX should naturally be compared to the RPAE in order to single out nonlocal effects. In order to compare to the RPAXC, we have considered a fourth approximation which we shall denote by RPAEC in which the exchange interaction is treated exactly as in the RPAE, but the correlation interaction is that of the RPAXC.

An important point should be underlined. The RPA method takes into account correlations not only in the excited states through the $A_{ma,nb}$ matrix elements but also in the ground state through the $B_{ma,nb}$ matrix elements. If HF orbitals are used in a many-body perturbation theory, then there are no single excitations in the first-order wave function and the double excitations are the leading terms of the correlation [26]. The RPAE thus corrects, in an unambiguous manner, the ground-state wave function by allowing for admixture of the two-particle–two-hole excitations to all orders. In the case of the LDA-RPA, some ambiguity remains since most of the correlations that are contained in the effective interaction are of RPA nature leading to a double counting uncertainty.

C. Sum rules

Beyond accounting for a large class of correlations, a major virtue of the random-phase approximation is its ability to satisfy sum rules exactly. Given the complete oscillator strength distribution, some of the moments,

$$S_q = \sum_k \omega_k^q f_k , \quad (3.16)$$

are related to simple ground-state properties. In the above expression, summation is understood as summation over the discrete states and integration over the continuum.

Starting from the jellium Hamiltonian of Eq. (2.1), the zeroth moment S_0, which measures the integral of the f distribution, equals the number of electrons (Thomas-Reiche-Kuhn sum rule). It is well known that this sum rule is violated in the Hartree-Fock approximation since a nonlocal potential leads to the breakdown of the equivalence of momentum and velocity. It is possible to show [30] analytically that the RPAE restores the Thomas-Reiche-Kuhn sum rule.

From a calculation of the S_2 moment with the jellium Hamiltonian, one shows [31] that the mean square frequency $\langle\omega^2\rangle = S_2/S_0$ is exactly given by the overlap integral of the positive ionic charge distribution and the exact ground-state electronic distribution, $\rho_e(\mathbf{r})$. With the jellium sphere of radius R, it can be expressed as

$$\langle\omega^2\rangle = \frac{4\pi\rho_0}{3}\left[1 - \frac{1}{Z}\int_R^\infty \rho_e(\mathbf{r})d\mathbf{r}\right] . \quad (3.17)$$

The first term is the square of the classical Mie frequency ω_M that characterizes the response of a small metallic sphere of constant density, ρ_0, to an ac dipole field and which is related to the plasma frequency by

$$\omega_M = \frac{\omega_p}{\sqrt{3}} = \frac{1}{r_S^{3/2}} . \quad (3.18)$$

The rms frequency for a quantal metallic jellium sphere is thus exactly related to the Mie frequency by

$$\sqrt{\langle\omega^2\rangle} = \omega_M\left[1 - \frac{\Delta Z}{Z}\right]^{\frac{1}{2}} , \quad (3.19)$$

where the ratio $\frac{\Delta Z}{Z}$ measures the fraction of electrons in the ground state that are outside the jellium sphere. This ratio vanishes in the classical limit. In terms of the spillout length defined by Eq. (2.11) and given in Table IV the rms frequency is expressed as

$$\sqrt{\langle\omega^2\rangle} = \omega_M\left[1 - \frac{3\delta_e}{R}\right]^{\frac{1}{2}} . \quad (3.20)$$

D. Results and comparisons

A numerical solution of the eigenvalue problem (3.10) requires a complete set of single-particle states. Clearly this matrix approach is simplified when dealing with discrete states only. In order to discretize the continuum states, it is convenient to confine the cluster to a cavity of finite radius. By choosing this cavity radius sufficiently large, the low-lying bound states in the cavity can

be brought arbitrarily close to the actual model bound states. Although the cavity spectrum is discrete, it is infinite. A finite model pseudospectrum is built by expanding the model orbitals in terms of a finite number of B splines. The low-lying states in this pseudospectrum can be adjusted very accurately to the model states by an appropriate choice of the number and order of the B splines used. For more details see Ref. [32]. An angular reduction of the RPA equation is performed with the restriction to dipole excitations. An external electric dipole field gives rise to a set of excitation channels. The radial amplitudes which are associated with these channels are expanded in terms of the pseudostates. In order to reach a very high accuracy, 50 B splines of order 7 have been used. As an example, we have ten channels for $Z = 40$, resulting in matrices A and B each of dimension 466×466. Note that in all our calculations the Thomas-Reiche-Kuhn f sum rule, $\sum_k f_k = Z$, is satisfied to better than one part in 10^5, providing a numerical test of the RPA calculations.

The oscillator-strength distributions have been calculated for closed-shell systems of 8, 18, 20, 34, 40, 58, 92, 134, and 196 electrons with the Wigner-Seitz radius parameter being fixed to $4a_0$ (sodium clusters). Matrix RPA calculations are shown in Figs. 3 and 4. The oscillator-strength distribution is in all cases bunched in a narrow energy range centered around the frequency of the collective dipole oscillation of the electron density with respect to the ionic background. One may interpret the f spectrum as resulting from the interaction between the collective mode and the particle-hole excitations of the same angular symmetry (1^-). Due to the long range nature of the Coulomb interaction, there is indeed a strong coupling between particle-hole excitations to build up the collective state.

The RPAE prediction (first column of Figs. 3 and 4) is compared to the RPAX prediction (second column). The RPAX systematically leads to a more fragmented f distribution than the RPAE, to which it is the local approximation. This trend is of course much more apparent for the smallest sizes. In Fig. 5, we show the density of natural parity dipole states obtained in the RPA calculations with our various treatments of the residual interaction. The different approximations lead to quite

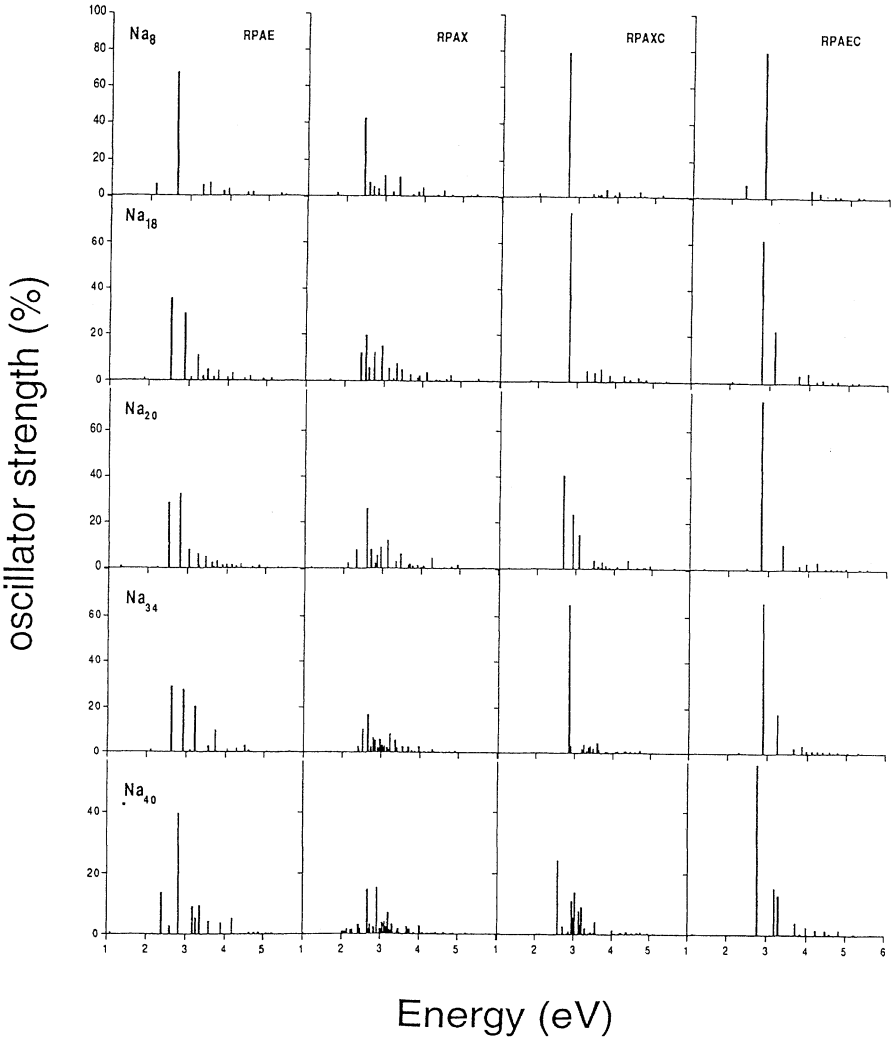

FIG. 3. Oscillator-strength distribution, calculated in the jellium RPAE, RPAX, RPAXC, and RPAEC, expressed as a percentage of the Thomas-Reiche-Kuhn sum rule given as a function of the excitation energy for closed-shell jellium clusters with $Z = 8$, 18, 20, 34, 40 delocalized electrons ($r_S = 4a_0$, sodium).

different spectra. The RPAX dipole spectrum is much denser than the correspondingly exact RPAE spectrum; this results from the fact, which we discussed previously, that the LDAX mean-field potential is shallower than the HF mean field. The collective state would, therefore, fragment into a large number of particle-hole excitations when the true exchange interaction is replaced by its local-density approximation. The comparison of the RPAEC and RPAXC densities of states, both containing the density-dependent correlation interaction, leads to the same conclusion. It is worth emphasizing that the collective dipole frequency (around 3 eV) is in a region of relatively low density of states thus implying important finite-size quantal effects. One observes that the RPAXC, which is commonly used by other practitioners [11–13], yields a density of dipole states that is quite close to the RPAE one. This agreement is of course accidental since the correlations contained in both methods are different. With regard to the RPAE and RPAX oscillator-strength spectra, the inclusion of the correlation term, RPAXC (third column of Figs. 3 and 4) and RPAEC (fourth column), results in a systematic narrowing of the f distribution and to the concentration of the force in essentially one line for the smaller systems (8 and 18).

The present RPAXC distributions should agree exactly with those already calculated by Yannouleas and co-workers [11–13] using the same exchange-correlation functional. We note, however, some differences in the positions of the main peaks but also different fragmentation patterns in some cases. For instance, the Na_{20} cluster was found [11] to optically respond at essentially two frequencies (2.6 and 2.9 eV) with about the same strength (35% of the total strength). Our present RPAXC calculation yields, for the same cluster, an f distribution that essentially splits into three lines at 2.67, 2.92, and 3.09 eV with 41%, 22%, and 13% strength, respectively. In order to check the numerical accuracy of the continuum discretization method, we compare the present matrix RPA to the TDLDA calculations using the same residual interaction. In the practical TDLDA calculations, it is necessary to add to the energy ω an imaginary part ($i\Gamma$) thus changing the δ functions into Lorentzians of width 2Γ. The numerical value of Γ was set equal to 8 meV, a value small enough to resolve the fragmentation of the

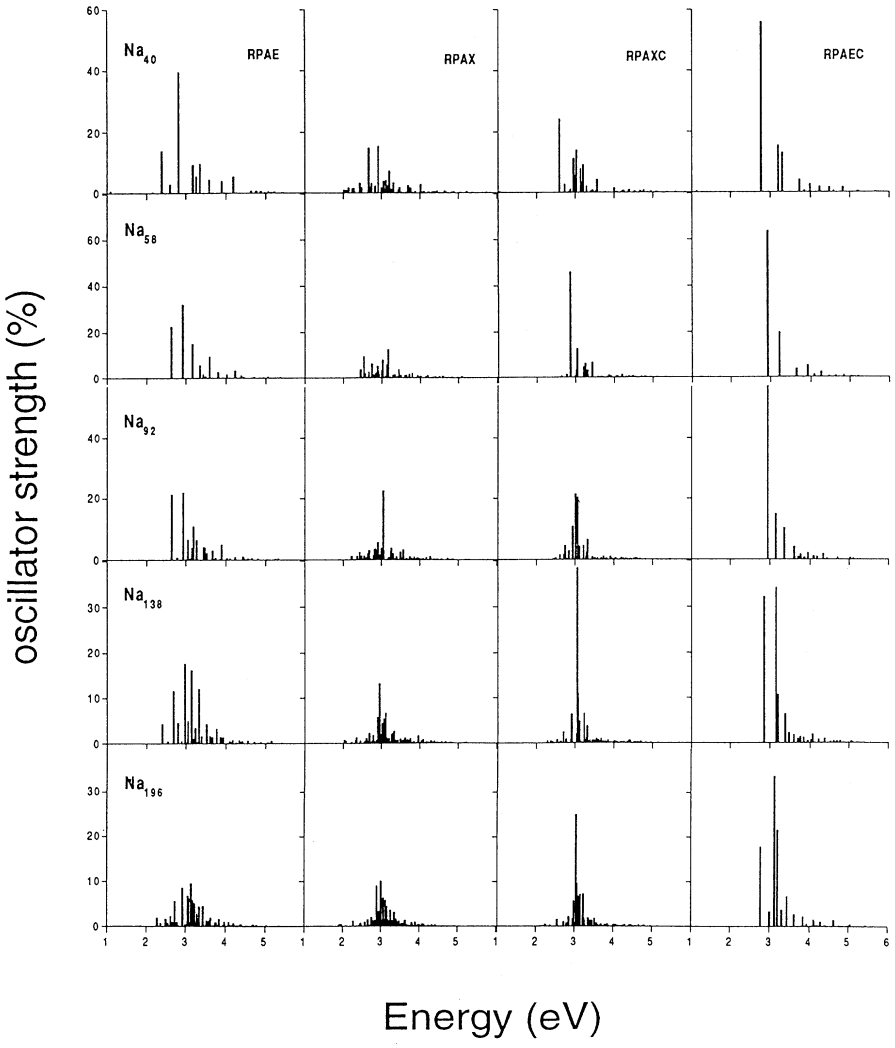

FIG. 4. Oscillator-strength distribution, calculated in the jellium RPAE, RPAX, RPAXC, and RPAEC, expressed as a percentage of the Thomas-Reiche-Kuhn sum rule given as a function of the excitation energy for closed-shell jellium clusters with $Z = 40$, 58, 92, 134, and 196 delocalized electrons ($r_S = 4a_0$, sodium).

oscillator-strength distribution. For all systems, a perfect agreement between the two methods has been met. The case of Na_{58} is given as an example in Fig. 6. The continuous TDLDA(XC) response shows the same spectral structure as the RPAXC discrete oscillator-strength distribution. We note that the latter differs in the relative intensities of the peaks from the one calculated in Ref. [13].

The finite-size effects are rapidly washed out when comparing various moments of the f distribution. In Fig. 7, the rms frequency obtained from the second S_2 moment is plotted against the size parameter, $n^{-1/3}$. The sum rule given by Eq. (3.17) is fulfilled in all cases to an accuracy of about one part in 10^3, thus providing another numerical test of the calculations. A linear fit to the calculated values numerically confirms that the asymptotic value is indeed the Mie frequency (3.4 eV in the present case), whatever the approximation under consideration. The essential lesson of Fig. 7 is that the various RPA approximations yield rms frequencies that differ by less than a few percent, a fact that arises from the sum-

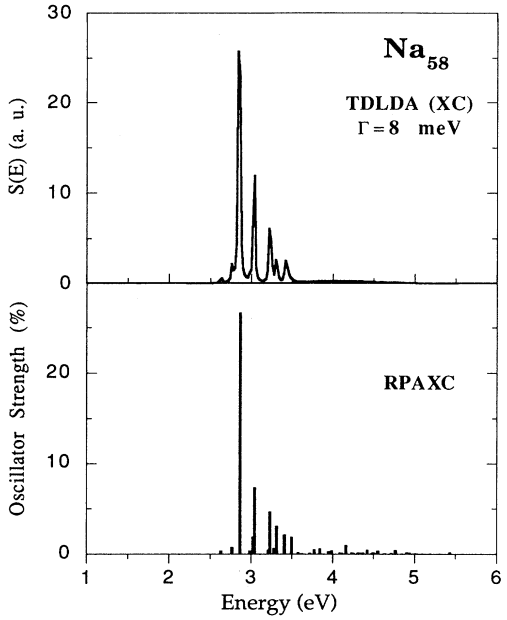

FIG. 6. Bottom panel: Oscillator-strength distribution of Na_{58} ($r_S = 4a_0$) from the matrix RPAXC calculation. Top panel: Arbitrarily normalized photoabsorption spectrum from the Green function TDLDA calculation.

rule constraints and very similar ground-state densities. The systematic (although tiny) discrepancies are reflecting the minute differences in the spillout lengths of the ground-state densities.

The mean frequency, obtained from the S_1 moment, $\langle\omega\rangle = S_1/S_0$ carries information on the the two-electron correlations in the ground state. Consequently, we could expect the various RPA approximations to lead to some extra discrepancies beyond the spillout effects. This is

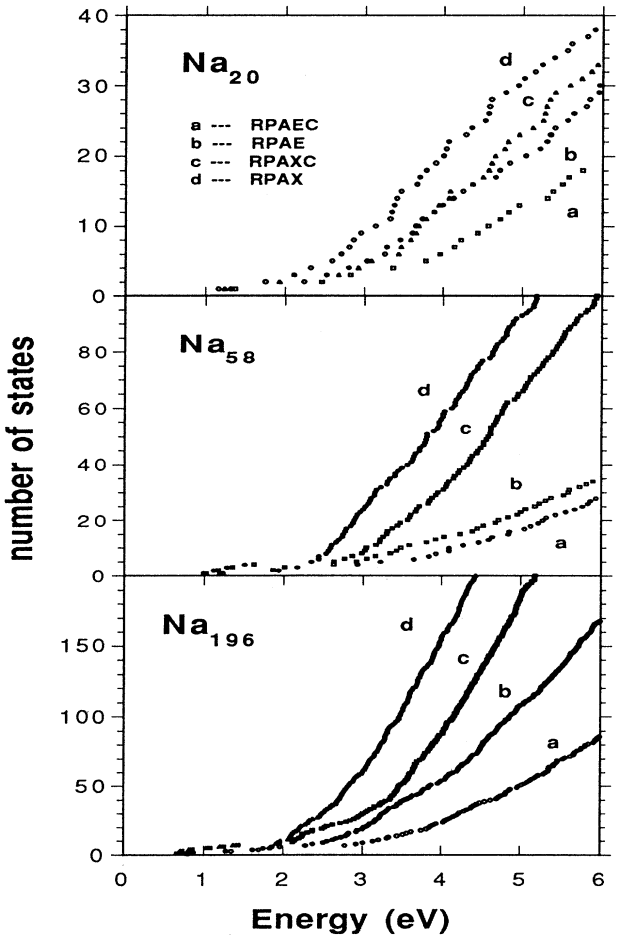

FIG. 5. Cumulated number of dipole excited states as a function of the excitation energy, calculated in the jellium RPAE, RPAX, RPAEC, and RPAXC, for jellium clusters with $Z = 20$, 58, and 196 delocalized electrons ($r_S = 4a_0$, sodium).

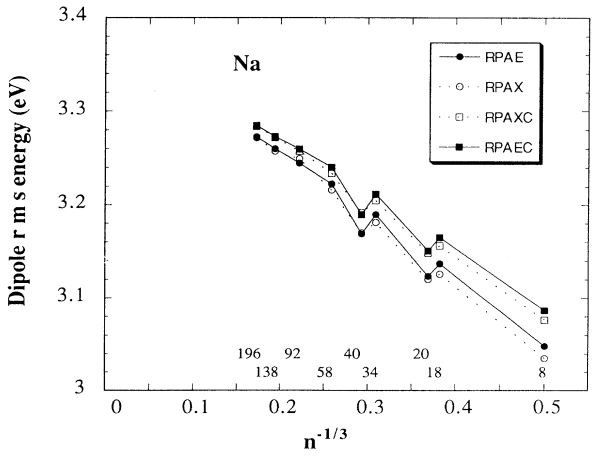

FIG. 7. Dipole absorption rms frequencies, calculated in the jellium RPAE, RPAX, RPAEC, and RPAXC, of closed-shell jellium clusters with 8, 18, 20, 34, 40, 58, 92, 138, and 196 particles, respectively, as a function of size ($r_S = 4a_0$, sodium).

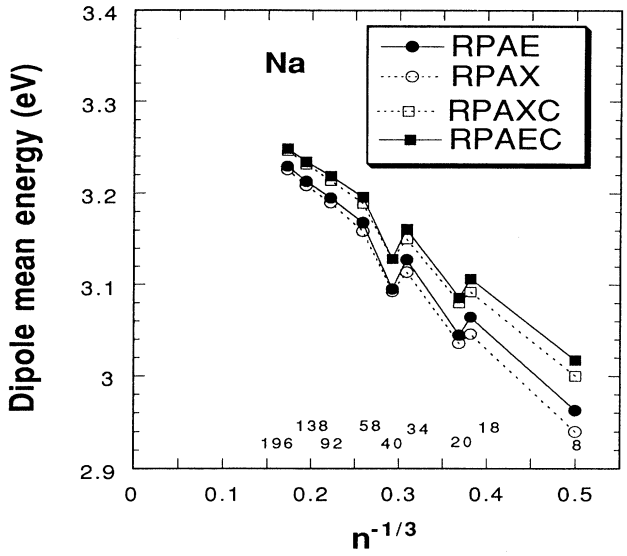

FIG. 8. Dipole absorption mean energies, calculated in the jellium RPAE, RPAX, RPAEC, and RPAXC, of closed-shell jellium clusters with 8, 18, 20, 34, 40, 58, 92, 138, and 196 particles, respectively, as a function of size ($r_S = 4a_0$, sodium).

indeed the case, although the effects are very small as shown by Figs. 8 and 9, where the mean values and the standard deviations, respectively, have been plotted against $n^{-1/3}$. The closed-shell jellium systems exhibit an optical response which is so compact that sum-rule constraints determine the major features.

Although the object of the present work is not a systematic confrontation between theory and the measured photoabsorption cross sections, we show as an illustration of the quality of the jellium approximation, a comparison between experimental data and the RPAE prediction in Fig. 10. The RPAE cross section has been obtained after convoluting the oscillator-strength distribution with Lorentzian shapes, centered at each discrete line, and with widths $\Gamma_k = 0.1\omega_k$. This convolution procedure models the coupling of the electronic density fluctuations to the ionic vibrations which is very likely the main cause of broadening of the lines [33]. The resulting photoabsorption spectra calculated for Na_{41}^+, Na_{59}^+, and Na_{93}^+ are reported in Fig. 10 and compared to experimental cross sections [6]. The agreement is surprisingly satisfactory. The theoretical cross section lies at a slightly higher energy than the measured one, and the overall shape is well

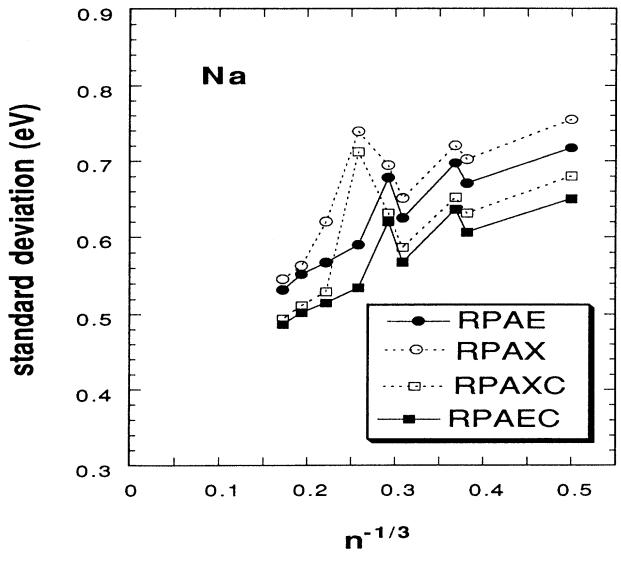

FIG. 9. Standard deviations of dipole absorption energies, calculated in the jellium RPAE, RPAX, RPAEC, and RPAXC, of closed-shell jellium clusters with 8, 18, 20, 34, 40, 58, 92, 138, and 196 particles, respectively, as a function of size ($r_S = 4a_0$, sodium).

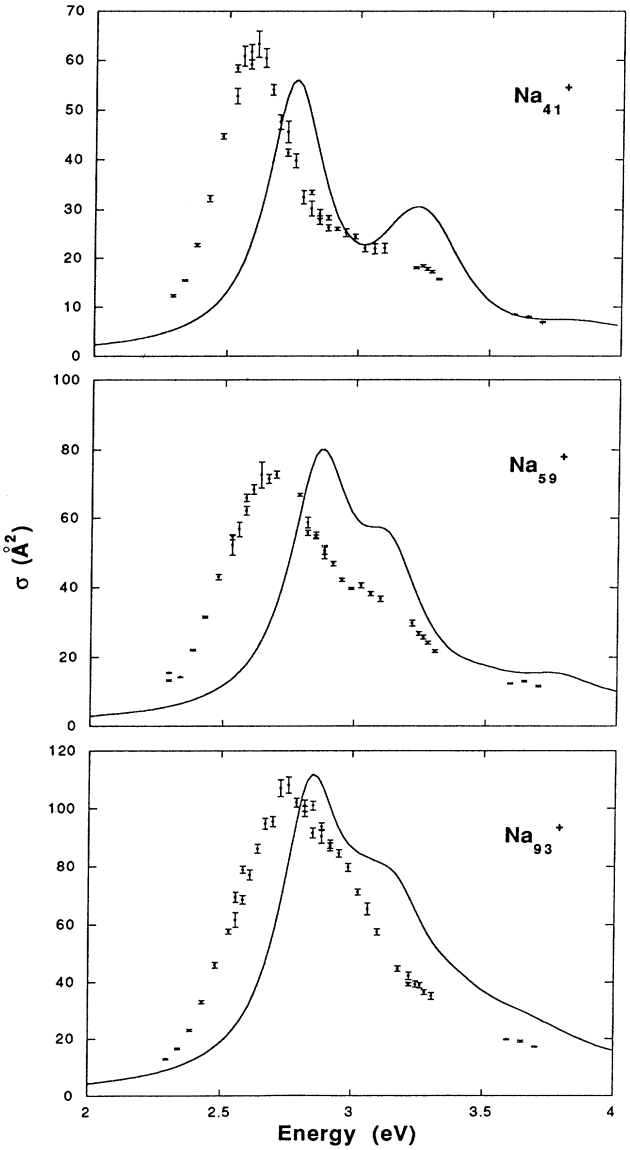

FIG. 10. Photoabsorption spectra, calculated in the jellium RPAE, of Na_{41}^+, Na_{59}^+, and Na_{93}^+ ($r_S = 4a_0$). The experimental cross sections are from Ref. [6].

reproduced. Keep in mind, however, that the fair agreement seen here for Na clusters collapses for Li clusters [3,34,35].

The static dipole polarizabilities are immediately obtained from the inverse squared, S_{-2} moment of the RPA oscillator-strength distributions. Here again, the predictions from four different residual interactions are very close to each other, as can be seen in Fig. 11 and in Table V. Only for the lighter systems (8, 18, 20) do the local-density approximations yield polarizabilities larger than those given by the correspondingly exact exchange calculations. This again reflects ground-state density distributions. If a single line were picking up the entire oscillator strength, then the static polarizability would be expressed as

$$\alpha = R^3 \left[1 + 3\frac{\delta_e}{r_s} n^{-\frac{1}{3}} \right] , \tag{3.21}$$

a trend which is fairly well satisfied by the present RPA calculations, although the slope is actually larger. The main correction with regard to the classical polarizability of the corresponding perfectly conducting sphere (R^3) is thus provided by the electron spillout in the ground state. As discussed previously, the LDAX predicts a density distribution that extends further outward than in the HF scheme, even though the asymptotic local potential falls off more rapidly, and thus yields a larger polarizability. The LDAXC that includes attractive correlations in the ground state gives a smaller spillout (see Table IV) than the the LDAX and, accordingly, the RPAXC polarizability is smaller than the RPAX one. One should note that the excellent agreement between the RPAXC and the TDLDA predictions is a confirmation of the accuracy

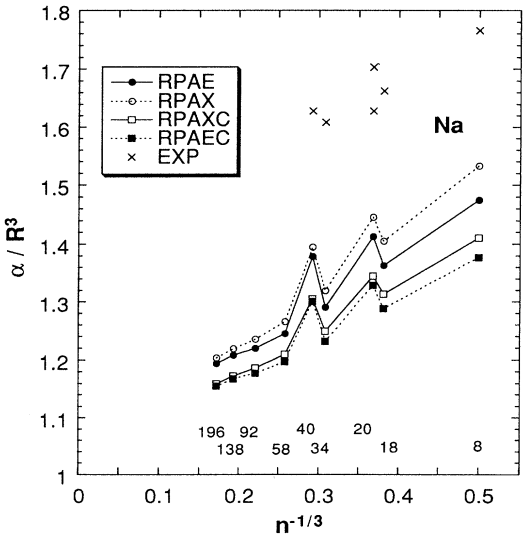

FIG. 11. Static polarizability, calculated in the jellium RPAE, RPAX, RPAEC, and RPAXC, of closed-shell jellium clusters with 8, 18, 20, 34, 40, 58, 92, 138, and 196 particles, respectively, as a function of size. ($r_S = 4a_0$, sodium). Experimental values [36] are indicated by crosses.

TABLE V. Static dipole polarizabilities (a_0^3) of Na clusters ($r_S = 4a_0$) for different sizes A, calculated in the RPA with various approximations for exchange and correlation: Exact exchange, α_{RPAE}; exact exchange and local correlation, α_{RPAEC}; local exchange only, α_{RPAX} and local exchange correlation, α_{RPAXC}. Predictions within the TDLDA-XC are also given, α_{TDLDA}. See text.

$A =$	8	18	20	34	40	58	92	138	196
α_{RPAE}	755	1570	1808	2806	3529	4619	7178	10667	14966
α_{RPAX}	784	1618	1850	2870	3570	4695	7270	10763	15089
α_{RPAXC}	722	1512	1721	2717	3339	4487	6981	10353	14541
α_{TDLDA}	722	1512	1721	2717	3340	4487	6981	10355	14543
α_{RPAEC}	705	1483	1701	2679	3328	4441	6930	10307	14484

of the present numerical methods. A comparison with experimentally measured polarizabilities [36], shows that the present predictions are systematically lower by about 30%, a shift which is much larger than the internal theoretical discrepancies. We believe that the explanation of this shift lies beyond the present jellium model and requires us to take into account ionic structure effects [34,31]. Further measurements on different and larger alkali-metal clusters should definitely be useful.

IV. CONCLUSION

The present work is aimed at systematically comparing local-density approximations to an exact treatment of exchange. The comparison is carried out within the jellium model applied to alkali-metal clusters, i.e., for rather homogeneous electronic densities. On one hand, it is shown that the ground-state densities given in the Hartree-Fock approximation and in the local-density-dependent approximation are very close to each other, except in the inner part of the cluster. The inclusion of a density-dependent correlation term does not modify much this density.

A density parameter of major importance for the optical response of the jellium systems is the fraction of electrons spilling out of the uniform positively-charged sphere; this parameter varies only slightly with the residual interactions considered in this work. Consequently, the rms values of the optical absorption frequencies given by the corresponding RPA models are also in close agreement.

The major differences between the local approximation and the exact treatment of exchange lie in the fragmentation of the oscillator-strength distribution as a consequence of quite different mean fields yielding different densities of natural parity dipole states. Therefore, whereas average values are rather model independent and basically constrained by sum rules, precautions must be taken when looking at the fine structure of the optical spectra, which indeed is model dependent. Moreover, the experimentally observed fragmentation is sensitive to the further details of the ionic structure not embraced by present jellium models.

ACKNOWLEDGMENTS

We would like to thank S.A. Blundell for many useful discussions. Clarifying discussions with G. Bertsch are particularly acknowledged. This work has been partially supported by SCIENCE Grant No. ERB-ESC-CT92-0770 of the European Communities. We thank the Institute for Nuclear Theory at the University of Washington for its hospitality and the Department of Energy for partial support during the completion of this work.

[1] For a review, see, W.A. de Heer, W.D. Knight, M.Y. Chou, and M.L. Cohen, Solid State Phys. **40**, 93 (1987); W.A. de Heer, Rev. Mod. Phys. **65**, 611 (1993).
[2] C. Bréchignac, P. Cahuzac, F. Carlier, and J. Leygnier, Phys. Rev. Lett. **63**, 1368 (1989).
[3] C. Bréchignac, Ph. Cahuzac, N. Kebaili, J. Leygnier, and A. Sarfati, Phys. Rev. Lett. **68**, 3916 (1992).
[4] K. Selby, V. Kresin, J. Masui, M. Vollmer, W.A. de Heer, A. Scheidemann, and W.D. Knight, Phys. Rev. B **43**, 4565 (1991).
[5] S. Pollack, C.R.C. Wang, and M.M. Kappes, J. Chem. Phys. **94**, 2496 (1991).
[6] Th. Reiners, W. Orlik, Ch. Ellert, M. Schmidt, and H. Haberland, Chem. Phys. Lett. **215**, 357 (1993).
[7] J. Borggreen, P. Chowdury, L. Lundsberg-Nielsen, K. Lützenkirchen, M.B. Nielsen, J. Pedersen, and H.D. Rasmussen, Phys. Rev. B **48**, 17 507 (1993).
[8] A. Zangwill and P. Soven, Phys. Rev. A **21**, 1561 (1980).
[9] W. Ekardt, Phys. Rev. B **31**, 6360 (1985).
[10] D.E. Beck, Phys. Rev. B **35**, 7325 (1987).
[11] C. Yannouleas, R.A. Broglia, M. Brack, and P.F. Bortignon, Phys. Rev. Lett. **63**, 255 (1989).
[12] C. Yannouleas and R.A. Broglia, Phys. Rev. A **44**, 5793 (1991).
[13] C. Yannouleas, E. Vigezzi, and R.A. Broglia, Phys. Rev. B **47**, 9849 (1993).
[14] C. Guet and W.R. Johnson, Phys. Rev. B **45**, 11 283 (1992).
[15] M. Brack, Phys. Rev. B **39**, 3533 (1989).
[16] P.G. Reinhard, M. Brack, and O. Gensken, Phys. Rev. A **41**, 5568 (1990).
[17] J.P. Perdew and A. Zunger, Phys. Rev. B **237**, 5048 (1981).
[18] J.M. Pacheco and W. Ekardt, in *Physics and Chemistry of Small Clusters*, edited by P. Jena, B.K. Rao, and S.N. Khanna (Kluwer, Richmond, 1992), p. 983; Z. Phys. D **24**, 65 (1992).
[19] G.F. Bertsch, Comp. Phys. Commun. **60**, 247 (1990).
[20] P. Hohenberg and W. Kohn, Phys. Rev. B **136**, 864 (1984).
[21] M. Brack, Rev. Mod. Phys. **65**, 677 (1993), and references therein.
[22] O. Gunnarsson and B.I. Lundqvist, Phys. Rev. B **13**, 4274 (1976).
[23] J.C. Slater, Phys. Rev. **81**, 385 (1951).
[24] P. Stampfli and K.H. Bennemann, Phys. Rev. A **39**, 1007 (1989).
[25] M.S. Hansen and H. Nishioka, Z. Phys. D **28**, 73 (1992).
[26] C. Guet, W.R. Johnson, and M. Madjet, Z. Phys. D **26**, S-125 (1993).
[27] S. Saito, S.B. Zhang, S.G. Louie, and M.L. Cohen, J. Phys. Condens. Matter **2**, 9041 (1990).
[28] M. Koskinen, P.O. Lipas, E. Hammaren, and M. Manninen, Phys. Rev. B **40**, 3643 (1989); Europhys. Lett. **19**, 165 (1992).
[29] D.J. Rowe, Rev. Mod. Phys. **40**, 153 (1968).
[30] M.Ya. Amusia and N.A. Cherepkov, Case Stud. At. Phys. **5**, 47 (1975).
[31] C. Guet, Comments At. Mol. Phys. (to be published).
[32] W.R. Johnson, S.A. Blundell, and J. Sapirstein, Phys. Rev. A **37**, 307 (1988).
[33] G.F. Bertsch and D. Tomanek, Phys. Rev. B **40**, 2749 (1989).
[34] S.A. Blundell and C. Guet, Z. Phys. D **28**, 73 (1992).
[35] Ll. Serra, G.B. Bachelet, Nguyen Van Giai, and E. Lipparini, Phys. Rev. B **48**, 14 708 (1993).
[36] W.D. Knight, K. Clemenger, W.A. de Heer, and W.A. Saunders, Phys. Rev. B **31**, 445 (1985).